Astron. Astrophys. 348, 261–270 (1999)

ASTRONOMY AND ASTROPHYSICS

EUV and radio observations of an equatorial coronal hole

F. Chiuderi Drago[1], **E. Landi**[1], **A. Fludra**[2], **and A. Kerdraon**[3]

[1] Department of Astronomy and Space Science, University of Florence, Italy
[2] Rutherford Appleton Laboratory, Chilton, Didcot, UK
[3] DASOP, Observatoire de Paris-Meudon, France

Received 22 April 1999 / Accepted 16 June 1999

Abstract. EUV and radio data of an equatorial coronal hole, observed in October 1996 at its central meridian transit, are compared. EUV lines were observed by the CDS instrument onboard SOHO and the radio emission by the Nancay Radioheliograph (France) in the frequency range 164–410 MHz.

Using the Differential Emission Measure (DEM), derived from EUV line intensities, we have computed the radio brightness temperature T_b, leaving the coronal temperature (upper limit of the DEM definition) and pressure as free parameters, to be determined from the comparison with the observations.

This analysis has shown that radio data, contrarily to EUV line intensities, cannot be fitted without the presence of isothermal plasma above the region where the DEM is defined, independently of the choice of parameters. A model, nicely fitting both sets of data, is derived, in which the coronal temperature and density are $T_c \leq 9 \times 10^5$ K and $N_e(0) \simeq 3 \times 10^8\, cm^{-3}$ respectively.

The assumption of hydrostatic equilibrium with a scale height derived from the electron temperature is discussed.

Key words: Sun: corona – Sun: radio radiation – Sun: UV radiation

1. Introduction

Coronal holes were first observed on X-ray plates by Underwood and Muney (1967), on EUV line spectroheliograms by Reeves and Parkinson (1970) and in white light by Altshuler and Perry (1972). They were then frequently observed during the Skylab Mission (1972–74) in the soft X-ray images and, about in the same years, also at metric wavelengths by Dulk and Sheridan (1974), Chiuderi Drago (1974), Lantos and Avignon (1975).

The aspect of coronal holes depends very much on the atmospheric level at which they are observed: coronal images, taken in all wavelength ranges listed above, show that coronal holes are much darker than the surrounding regions, they don't show up in the spectroheliograms taken in Transition Region lines (Munro and Withbroe, 1972) and they are brighter in the radio maps at mm-wavelengths (Kosugi et al. 1986).

Send offprint requests to: E.Landi (enricol@arcetri.astro.it)

The comparison between X-ray and metric wavelength observations of coronal holes, although very seldom done on the same hole, has evidenced a strong disagreement in the value of the coronal temperature T_c: all radio observations listed above indicate coronal temperatures of the order of $(8\text{–}9) \times 10^5$ K, while from X-ray observations electron temperatures larger than one million degrees are inferred. According to recent Yohkoh observations, $T_c(CH) \simeq 2 \times 10^6$ K (Hara et al. 1994). The impossibility to reconcile EUV and radio observations of the same equatorial coronal hole, was ascribed in the past to the presence of small scale unresolved inhomogeneities (Chiuderi Drago et al. 1977).

It must be pointed out, however, that recent observations of coronal holes, performed with the SOHO/CDS instrument seem to indicate that also EUV line intensities can be accounted for by assuming a coronal temperature lower than 10^6 K (Fludra et al. 1997, 1999a, 1999b; Del Zanna & Bromage 1997, David et al. 1998).

In the present work we compare radio and EUV observations of the $same$ coronal hole in order to determine with a better accuracy the plasma parameters both in the corona and in the Transition Region (TR). To this purpose we have compared the intensity of several EUV lines with the radio emission in the decimetric and metric range of wavelenths, both generated in this portion of the solar atmosphere.

Radio observations of polar coronal holes are difficult because the waves path in the solar corona is strongly bent at metric wavelengths, due to the variable refractive index, so that the inner corona around the limb cannot be observed and what we see in that position is the radiation coming from higher levels (see for instance Kundu, 1965).

Our comparison was therefore done on an equatorial coronal hole, observed on October 18 and 19, 1996 during its central meridian transit. The hole was observed by the CDS and EIT instruments onboard SOHO and by the Radioheliograph of Nançay (France) at four radiofrequencies between 169 and 410 MHz. CDS observations were taken on October 18, while radio observations refer to October 19.

EUV and Radio observations will be described in Sect. 2. The analysis of EUV lines observed by CDS, the method for the determination of the Differential Emission Measure (*DEM* $= N^2 dh/dT$) and of the radio brightness temperature are pre-

sented in Sect. 3. In Sect. 4 we present the comparison between EUV and radio data, performed using the *DEM* in the TR up to a certain temperature determined, together with the electron pressure at the basis of the corona, from the best fit of radio data. The best fitting models are then checked by computing the EUV line intensities.

A general discussion on the results is given in Sect. 5. Summary and conclusions are presented in Sect. 6.

2. Observations

2.1. EUV observations

The EUV spectra in the coronal hole were taken with the Coronal Diagnostic Spectrometer (CDS) on board of the SOHO satellite. The CDS is a spectrograph aimed to produce spectra of selected regions of the solar surface in six spectral windows of the extreme ultraviolet from 150 Å to 785 Å (Harrison et al. 1995). CDS is composed of two different instruments, namely the Grazing Incidence Spectrometer (GIS) and the Normal Incidence Spectrometer (NIS).

In the present work we have used only the data of the NIS instrument. The NIS operates in two spectral windows covering the 307–379 Å and 513–633 Å spectral range. Of the whole NIS spectral band, only selected portions have been observed, thus reducing the total observing time. The selected spectral windows allow to detect lines formed in a broad range of temperatures, from 10^4 K to 10^6 K, thus covering the whole range of temperature between chromosphere and corona. Also, the presence of density sensitive line pairs of O IV and Si IX allows to measure the electron density of the emitting plasma at transition region and coronal temperatures.

The data files are s5368r00 and s5369r00: the field of view of the s5368r00 file is located north of the other one, along the solar meridian, with only a partial overlapping. The field of view of each file is $122'' \times 240''$, giving a total field of view of $122'' \times 450''$, covering the central portion of the coronal hole.

The raw data have been cleaned from cosmic rays and calibrated using the standard routines available as part of the CDS software. A combined map of the observed region from the two data files at the wavelength of the Mg X 624.94 Å line, one of the hottest in the present dataset (the temperature of formation is $\sim 1 \times 10^6$ K) is displayed in Fig. 1. The structure of the coronal hole is evident at the center of the image as a dark lane sorrounded by the brighter quiet Sun plasma. The bright region visible at the bottom is the bright point visible also in in the EIT image shown in Fig. 2.

does The hole area has been identified with the region where $I_{624.94} < 10$ phot cm^{-2} s^{-1} arcsec^{-2} and the intensity of each line has been averaged within this area. The contour plot of the selected area is marked in Fig. 1.

The observed lines are listed in Table 1, together with their average intensity, I_{obs}, measured in units of phot cm^{-2} s^{-1} arcsec^{-2}, their uncertainty σ_I and the temperature of formation T_{eff} defined, consistently with Landi & Landini 1997, as:

Table 1. EUV spectral line intensities observed by CDS. Intensities are in phot cm^{-2} s^{-1} arcsec^{-2}. σ_I represents the experimental uncertainty.

Ion	λ (Å)	I_{obs}	σ_I	T_{eff}
Fe XI	341.113	0.6	0.1	9.84×10^5
Si IX	341.949	1.6	0.2	9.75×10^5
Mg VI	349.117	1.8	0.2	5.51×10^5
Mg VI	349.137			
Mg VI	349.168			
Mg VI	349.188			
Si IX	349.794	2.4	0.2	9.75×10^5
Si IX	349.873			
Mg VII	367.674	4.8	0.3	7.79×10^5
Mg VII	367.683			
Mg IX	368.070	27.5	0.6	9.68×10^5
Ne IV	543.892	3.9	0.1	2.00×10^5
O IV	553.329	13.0	0.6	1.84×10^5
O IV	554.075	22.5	1.6	1.84×10^5
O IV	554.513	62.8	1.8	1.84×10^5
O IV	555.262	14.0	0.6	1.84×10^5
Ca X	557.764	2.0	0.8	8.54×10^5
Ne VI	558.593	4.9	0.1	4.59×10^5
Ne VII	558.609			
Ne VI	562.711	7.9	0.2	4.59×10^5
Ne VI	562.803			
Ne V	572.027	4.4	0.2	3.31×10^5
Ne V	572.098			
Ne V	572.331			
Ca X	574.010	2.1	0.1	8.54×10^5
C III	574.280			7.92×10^4
He I	584.334	260.7	4.6	2.71×10^4
O III	599.597	26.1	0.5	1.09×10^5
He II	$2\times$303.780	61.3	0.9	1.04×10^5
He II	$2\times$303.786			
O IV	608.396	9.7	0.4	1.84×10^5
Mg X	624.941	5.2	0.1	9.91×10^5
O IV	625.852	0.7	0.2	1.84×10^5
O V	629.732	203.6	2.9	1.93×10^5

$$LogT_{eff} = \frac{\int g(T)\,\varphi(T)\,logT\,dT}{\int g(T)\,\varphi(T)\,dT} \quad (1)$$

2.2. Radio observations

The Nançay Radioheliograph (NRH) consists of 19 antennas with a minimum baseline of 50 m in the E-W direction and 24 antennas with a minimum baseline of 54.3 m in the N-S direction. The maximum baselines are 3200 m and 1248 m respectively (Kerdraon & Delouis 1997). This instrument supplies two dimensional maps of the Sun at five frequencies between 150 and 450 MHz. The frequencies at which the coronal hole of October 19, 1996 was observed are: 164 MHz, 236 MHz, 327 MHz and 410 MHz.

For details on the instrument performances and on the calibration techniques used see Kerdraon & Delouis 1997.

The time resolution of the NRH can be as high as one images every 0.1 seconds at each frequency and the angular resolution in the N-S and in the E-W directions depends, besides frequency,

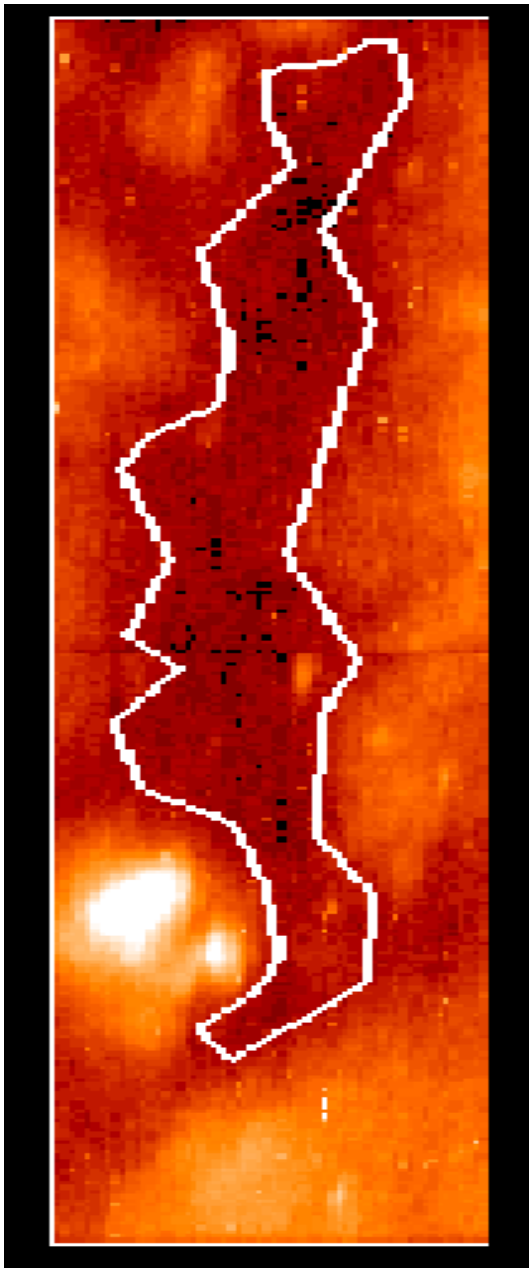

Fig. 1. Map of the coronal hole as seen in the Mg X 624.94 Å line. The contour plot indicates the portion of the image considered in the present study.

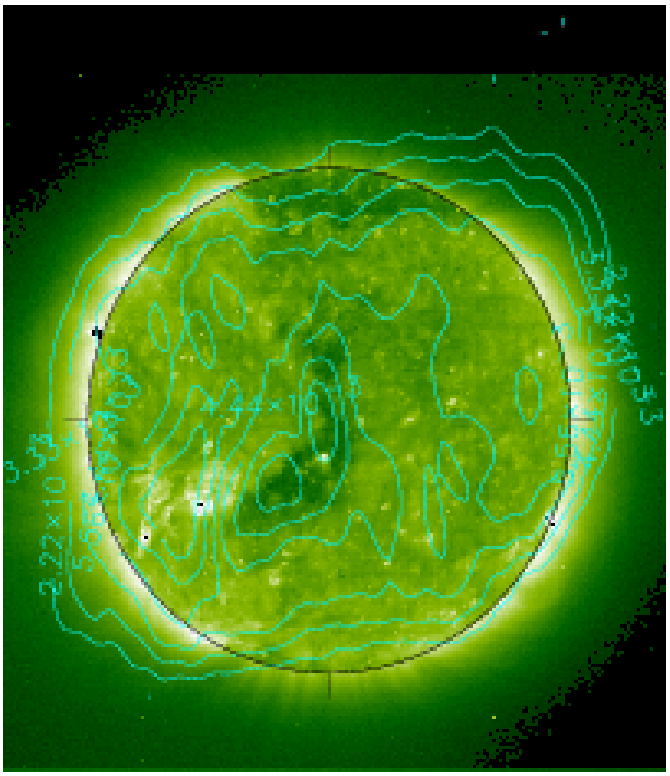

Fig. 2. Contours of radio brightness temperature at 410 MHz superimposed to the EIT image taken in the 195 Å filter at 21:00 UT; the small disalignement between the two images is due to the time difference between the observations ($\simeq 6^h$).

Table 2. Antenna beam width.

ν MHz	$M.A.$ arcmin	$m.A.$ arcmin
164	5.2	2.6
236	4.3	2.2
327	2.9	1.6
410	2.7	1.4

on the period of the year; moreover, during the day, the beam pattern changes size and rotates in the sky.

Since coronal holes are very stable structures, we have averaged the observations over several hours around the time when the major axis of the beam was roughly parallel to the axis of the southern portion of the coronal hole: this minimizes the contribution of surrounding regions to the hole brightness temperature. The considered radio brightness temperature will be in fact averaged over this wider portion of the coronal hole.

In Table 2 are reported, for the time of our observations, the major and minor axis (M.A. and m.A. respectively) of the ellipse representing the antenna beam at each frequency.

In Fig. 2 the radio contour plots at 410 MHz are overlaid on the EIT image of Fe XII line at 195 Å: the shape of the hole in the two ranges of wavelengths is very similar and the small disalignement is due to the time difference ($\simeq 6^h$) between the two observations.

The average width of the hole, between points where $I \sim I_{Q.S.}/2$ on the EIT image shown in Fig. 2 are: $\sim 1.5\ arcmin$ in the northern part and $\sim 2.4\ arcmin$ in the southern one, where the hole axis is tilted of about 50° with respect to the N-S direction.

If we compare the width of the hole with the minor axis of the beam area shown in Table 2, we find that the northern portion of the hole is narrower than the beam at all frequencies except at 410 MHz. In the southern part, where the hole is larger, its width is still smaller than the beam at 164 MHz, it has about the same size of the beam at 236 MHz and is definitly larger at 327 and 410 MHz. At these two latter frequencies two minima are

clearly seen in the radio maps separated by a region of higher T_b which corresponds to the bright point in the EIT images, very well visible in Fig. 1. At 236 and 164 MHz only one minimum is observed.

The T_b estimate in the hole has been therefore performed in the following way: we have first traced on each map several E-W scans across the disk: at all frequencies the brightness temperature shows a more or less pronounced minimum in the scans crossing the southern part of the hole. According to what previously said, at the lowest frequency, $\nu = 164$ MHz, we have considered the deepest of these minima as an upper limit of the T_b in the hole. At the two highest frequencies, where the southern part of the hole is resolved, we have calculated the average value of the minimum temperature of all scans across this part except that corresponding to the bright point. Finally, at 236 MHz, we have measured both the lowest minimum and the average one. The T_b values obtained in this way are plotted in Figs. 4 and 5.

The reliability of the T_b measurement at 164 MHz has been checked in the following way (Delouis, private comunication). A rectangular model of the hole has been assumed taking its width from the 410 MHz map and leaving the brightness temperature T_b at the bottom as a free parameter. This model has been convolved with the 164 MHz beam and the bottom T_b value which best reproduced the 164 MHz observations has been evaluated, obtaining $T_b = (8.8 \pm 0.5) \times 10^5$ K. This value must be compared with the upper limit $T_b < 9.0 \times 10^5$ K previously determined.

In general the calibration techniques described in Kerdraon & Delouis 1997 and the method for T_b determination used in the present work allow to measure radio brightness temperatures with an accuracy better than 5×10^4 K.

It must be pointed out that the radio brightness temperature has been averaged over the whole southern portion of the hole, mostly located south-east of the bright point, while EUV line intensities have been averaged only over the portion located north of the bright point (see Fig. 1). However a comparison between the two minima in the 410 MHz map, shown in Fig. 2 (the frequency where the maximum resolution is achieved) indicates that the difference of the two T_b is of the order of 15%, the southern minimum being deeper that the northern one.

The real difference between the two values is probably even smaller due to a possible contribution of the surrounding regions to the northern portion of the coronal hole.

The set of data obtained with this procedure are rather different from those previously presented by Chiuderi Drago et al. 1999, due to a better accuracy in handling the radio data.

3. Data analysis

3.1. DEM analysis with CDS

The line intensities reported in Table 1 have been used to determine the coronal hole *DEM*, defined as

$$\varphi(T) = N_e^2 \frac{dh}{dT} \tag{2}$$

Element abundances have been taken from Feldman et al. 1992 (coronal values). Ion fractions come from Arnaud & Raymond 1992 (Fe ions) and Arnaud & Rothenflug 1985 (other ions). To determine the *DEM* of the emitting plasma we used the iterative method described by Landi & Landini 1997 to which we refer for details.

The *DEM* curve is usually defined in a temperature range including plasma from chromospheric to coronal conditions; above the coronal temperature, where no more lines are detected by the instruments, the *DEM* function is very often extrapolated to a very low value at a very high temperature ($\sim 10^8$ K). This causes the *DEM* to have a sharp maximum around the coronal temperature. Landi & Landini 1998 have criticized this assumption, since a decreasing *DEM* at high temperatures implies an increasing temperature gradient $\frac{dT}{dh}$, which would produce a physically unacceptable high temperature. It would also pose problems to the energy balance equations, because the temperature gradient is linked to the heat conductive flux. Consequently, Landi & Landini 1998 proposed to truncate the *DEM* at a *maximum temperature* T_{max} beyond which the *DEM* is not defined; in this way $\frac{dT}{dh}$ does not increase when the temperature approaches T_{max}.

In this paper we will use both methods to determine the *DEM* from the observed EUV line intensities in the coronal hole. These *DEM* curves will be then tested by computing the radio brightness temperature and comparing it with the observations.

The *DEM* fits are displayed in Fig. 3 together with the data points. It must be pointed out that, in the data points plotted in the figure, the Fe, Mg and Si abundances from Feldman 1992 have been lowered by a factors ranging from 3.4 to 4.0, getting a good agreement with the Grevesse & Anders 1991 photospheric values. This indicates that the First Ionization Potential effect (FIP effect – see e.g. Haisch et al. 1996) cannot be applied to this dataset, in agreement with the findings of Del Zanna & Bromage 1999.

The strong peak in the *DEM* curve displayed in Fig. 3 (left) occurs at temperatures slightly smaller than 10^6 K, while the *DEM* curve displayed in Fig. 3 (right) is defined up to $T_{max} = 10^6$ K.

3.2. Radio brightness temperature

The radio brightness temperature T_b is related to the plasma parameters through the transfer equation:

$$T_b = \int_0^{\tau_{max}} T\, e^{-\tau}\, d\tau \tag{3}$$

where

$$d\tau = -\frac{0.2 N_e^2 dl}{\nu^2\, n\, T^{3/2}} \tag{4}$$

is the differential radio optical depth. In this equation l is the coordinate along the ray path and n is the refractive index:

$$n = \sqrt{1 - (N_e/N_{cr})} \tag{5}$$

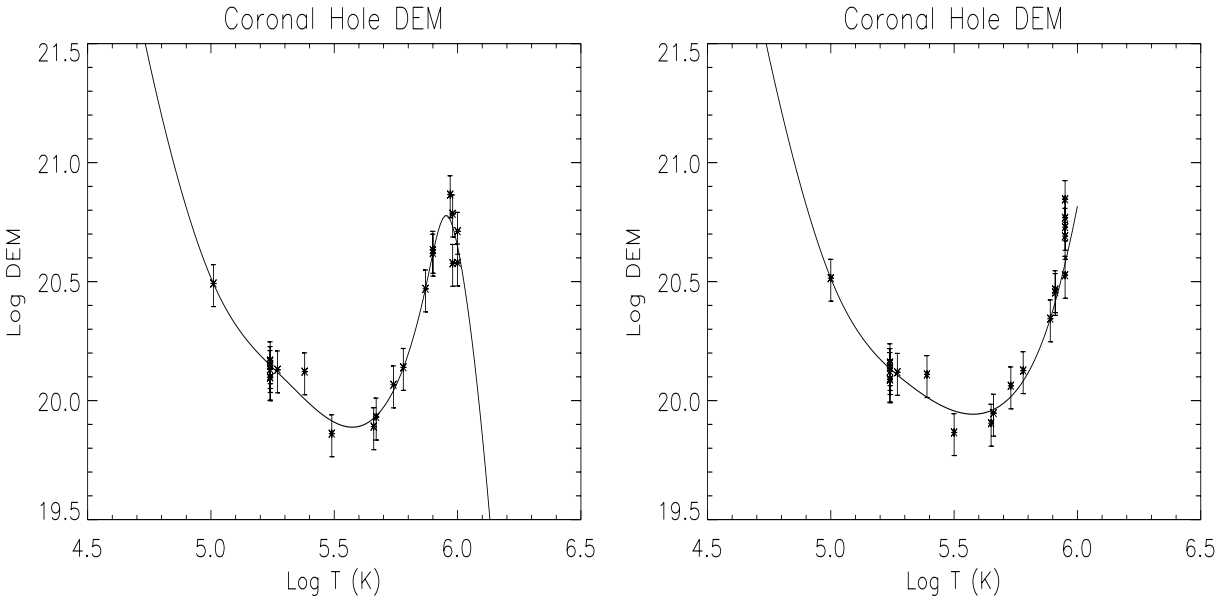

Fig. 3. *DEM* for the coronal hole region. *Left*: usual definition for the *DEM*. *Right*: *DEM* truncated at $T_{max} = 10^6$ according to Landi & Landini 1998. Experimental *DEM* constrains provided by each observed line are overplotted on the *DEM*.

where $N_{cr} = 1.24 \times 10^{-8}\ \nu^2$ is the critical density. Since the coronal hole is located near the disk center, the ray path is a straight line, $N_e^2 dl \simeq N_e^2 dh$ and Eq. 4 may be re-written as

$$d\tau = -\frac{0.2\varphi(T)}{\nu^2\ n\ T^{3/2}}\ dT \tag{6}$$

τ_{max} is the optical depth of the level where $N_e = N_{cr}$ and $T = T_{cr}$. At very short wavelengths, where the refractive index $n \simeq 1$ in the TR and corona, T_b can be directly derived from the EUV lines intensity through the *DEM* without any further assumption and the integral in Eq. 3 is performed up to $\tau >> 1$

At the frequencies considered in this paper this approximation does not hold, as the critical density is located in the high TR or in the corona.

In order to take into account the refractive index n in Eq. 4, we must know the electron density profile in the upper part of the solar atmosphere. This has been done in the two following ways:

- *(a)* from the simple assumption of a constant electron pressure in the TR (hereafter defined as $p = N_e T$), getting $N_e(T) = p_0/T$
- *(b)* by combining the *DEM* profile with the assumption of the hydrostatic equilibrium:

  $$N_e dT + T dN_e = -\alpha N_e dh \tag{7}$$

  getting

  $$N_e^2(T) = T^{-2} \times \left(C - 2\alpha \int_{T_0}^{T} T\ \varphi(T)\ dT \right) \tag{8}$$

  where $\alpha = \frac{\mu m_H g_\odot}{k_B} \simeq 1.98 \times 10^{-4}$ K cm $^{-1}$ and C is an integration constant related to the electron pressure at the temperature T_0: $C = p^2(T_0)$.

The lower temperature in the above integral has been arbitrarily set $T_0 = 5 \times 10^4$ K: this value does not affect the calculations since all considered radio frequencies have their critical level at temperature $T_{cr} \gg T_0$ and therefore the integral of the transfer equation stops at higher temperature.

For every value of T_{max}, used as an upper limit of the integral in Eq. 8, there exists a corresponding minimum value of the electron pressure p_{min}, given by

$$p_{min}^2 = 2\alpha \int_{T_0}^{T_{max}} T\ \varphi(T)\ dT \tag{9}$$

Pressure values lower than p_{min} would give $N^2 < 0$ at $T \leq T_{max}$.

4. Comparison between EUV and radio observations

The radio brightness temperatures have been computed from Eqs. 3 and 4, by substituting $N_e^2 dl \simeq N_e^2 dh$ with $\varphi(T)dT$ and using $N_e(T)$, derived from the assumptions (a) and (b) mentioned above, in the refraction undex. Both the *DEM* functions displayed in Fig. 3 have been used in the calculation.

No substantial difference is found between the results obtained using the two density profiles (*a*) and (*b*) mentioned above. This is because the electron density only enters the refractive index. In the following we will therefore show only the results obtained using the hydrostatic equilibrium assumption, mentioning the other ones when necessary. The assumption of hydrostatic equilibrium in a coronal hole will be discussed in the next section.

Fig. 4 displays the radio brightness temperatures calculated using both the *DEM* curves reported in Fig. 3 and three values of the electron pressure p_0. The results obtained using the standard *DEM* definition show a rather good agreement with the

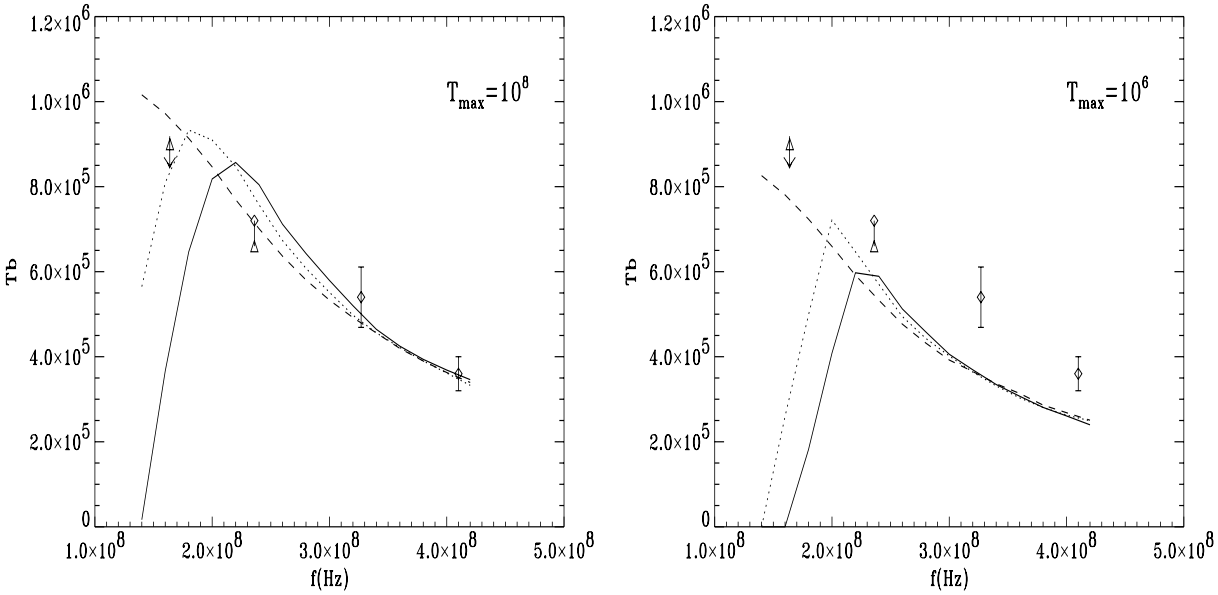

Fig. 4. Comparison between computed and observed radio brightness temperature. Values of p_0 are 3×10^{14} (dashed line), 4×10^{14} (dotted line) and 5×10^{14} (full line) cm^{-3} K^{-1}. *Left*: standard *DEM* definition (up to 10^8 K); *Right*: Landi & Landini 1998 *DEM* definition, truncated at $T_{max} = 10^6$ K.

observations at high frequencies, where the curves are almost independent of p_0. At low frequencies, on the contrary, the curves exceed the observed T_b and, moreover, they present a cut-off at a frequency decreasing with decreasing electron pressure.

It could therefore appear that a good agreement with the observations could be found in the whole observed range of wavelengths, by decreasing furthermore the electron pressure. However an electron pressure lower than 3×10^{14} cm^{-3} K^{-1} leads to $N_e^2 < 0$ at $T < 10^8$ K and is therefore unacceptable.

The results obtained using the Landi & Landini 1998 *DEM* curve show the same problem of the cut-off at low frequencies. Moreover the computed T_b are lower than the observed ones in the whole frequency range and it is clear, from the trend of the curves, that there are no values of the electron pressure p_0 able to provide radio brightness temperatures in agreement with the observations.

The reason of this disagreement is due, in our opinion, to have neglected the presence of an isothermal corona at the top of the TR. In the derivation of the DEM from EUV line intensities, the presence of an isothermal corona is in fact not properly considered as the coronal contribution to the intensity of EUV lines formed at temperatures close to T_{max} is included in the *DEM*.

The density profiles derived from the *DEM*, irrespective to the adopted assumption on the electron pressure trend, are therefore abruptly truncated at $T = T_{max}$. If the value of the electron density at $T = T_{max}$, which depends on the assumed value of electron pressure, turns out to be larger than the critical density at a given frequency ν_0, no contribution to the T_b will be given by the atmosphere at all frequencies $\nu \leq \nu_0$, thus producing the sharp cut-off noticed in Fig. 4.

If, on the contrary, the presence of a nearly isothermal corona, where $dT/dh \simeq 0$ and hence the *DEM* cannot be defined, is assumed above the level where $T = T_{max}$, we have still an emitting plasma, whose density slowly decreases with height up to extremely low values, that can provide a non zero T_b at any frequency.

Having this in mind, we have repeated the calculations using the *DEM* up to $T = T_{max}$ and adding above this level an isothermal corona at $T_c = T_{max}$.

If hydrostatic equilibrium is assumed, the coronal radio optical depth τ_c can be analytically calculated obtaining:

$$\tau_c = \frac{0.27\ H\ N_{cr}^2}{\nu^2 \cdot T_c^{1.5}} \tag{10}$$

when the critical density is located in the corona ($N_{cr} < N_e(0)$) and

$$\tau_c = \frac{0.27\ H}{\nu^2 \cdot T_c^{1.5}} \times (2\sqrt{N_{cr} \cdot d}\,(d/3 - N_{cr}) + 4/3\ N_{cr}^2) \tag{11}$$

when the radiation crosses the whole corona ($N_{cr} > N_e(0)$). In the above equations $H = T_c/\alpha$ is the scale height, $d = N_{cr} - N_e(0)$ and $N_e(0)$ is the the electron density, derived from the assumed electron pressure trend, at $T = T_{max}$.

The electron pressure p_0 and the coronal temperature T_{max} (the upper limit of the integral in Eq. 8) are left as free parameters to be determined from the fit of radio data.

The fit of the radio spectrum has been done for three sample values of the coronal temperature, $T_c = 7.9{\times}10^5$, $8.9{\times}10^5$ and 1×10^6 K and several values of the electron pressure in the TR spanning from $2{\times}10^{14}$ to $5{\times}10^{14}$ cm^{-3} K. The results, obtained assuming the hydrostatic equilibrium in the whole considered portion of the atmosphere (assumption (*b*)) are compared with the observations in Fig. 5.

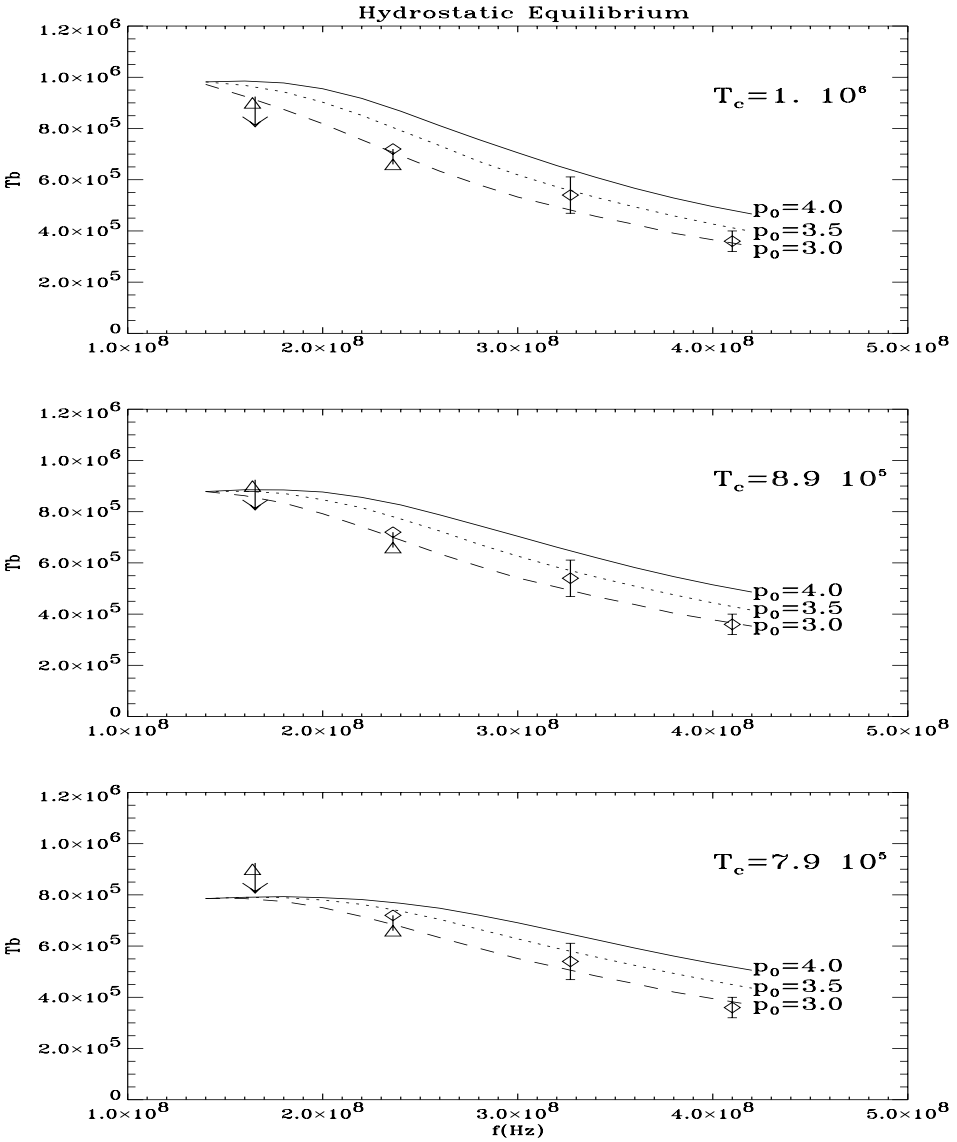

Fig. 5. Comparison between computed and observed radio brightness temperature,in the assumption of hydrostatic equilibrium. P_0 is the electron electron pressure at $T_0 = 5 \times 10^5$ K in units of 10^{14} cm^{-3} K.

Unfortunately the lack of resolution at 164 MHz does not allow a precise determination of the coronal temperature, but only an upper limit, $T_b \sim 9 \times 10^5$ K.

Very good fits are obtained for coronal temperatures $T_c \leq 8.9 \times 10^5$ K assuming a value of the electron pressure $p_0 = (3 \div 3.5) \times 10^{14}$ cm^{-3} K at $T_0 = 5 \times 10^4$ K. Identical results are obtained if a constant electron pressure (assumption (*a*)) is assumed in the TR with $p_0 = (2.5 \div 3) \times 10^{14}$ cm^{-3} K. It must be pointed out that an electron pressure $3\ (3.5) \times 10^{14}$ cm^{-3} K at $T_0 = 5 \times 10^4$ K, in the hydrostatic equilibrium assumption, leads to electron pressure values of $2.5\ (3) \times 10^{14}$ cm^{-3} K at $T = 8.9 \times 10^5$ K, thus indicating that the parameter affecting the radio data is the electron pressure at bottom of the corona and not its trend in the TR.

From these values of the coronal electron pressure the following electron densities are derived at the base of the corona: $N_e(0) = 3.00 \pm 0.30 \times 10^8$ cm^{-3} ($T_c = 8.9 \times 10^5$ K) and $N_e(0) = 3.40 \pm 0.30 \times 10^8$ cm^{-3} ($T_c = 7.9 \times 10^5$ K).

These values of the density can be compared with those obtained from density sensitive line ratios available in the dataset.

4.1. Density diagnostic

Electron densities have been measured at TR and coronal temperatures using the O IV 625.8/554.5 and Si IX 341.9/(349.8+349.9) line ratios: the theoretical ratios have been calculated using the CHIANTI database (Dere et al. 1997, Landi et al. 1999), taking into account the effects of photoexcitation from photospheric radiation, as described by Young et al. 1999.

The resulting density values are reported in Table 3, together with the electron pressure $p_e = N_e \times T_{eff}$ where T_{eff} is the temperature of ion formation given by Eq. 1.

It is interesting to note that neither the constant electron pressure nor hydrostatic equilibrium assumptions are satisfied by the data shown in the table, as the electron pressure varies by more than one order of magnitude between $T \sim 10^5$ K and $T \sim 10^6$ K, in conflict with our previous calculations.

Table 3. Electron density and pressure measurement for the coronal hole.

Ion	Log T_{eff}	Log N_e	Log P_e
O IV	5.2	10.10±0.20	15.36±0.20
Si IX	6.0	8.10±0.10	14.10±0.10

It must be pointed out however that the density determination from the O IV is quite uncertain because the line is weak and blended with the Mg X 624.94 Å , moreover its wavelength falls in a region of the detector where the calibration is rather uncertain (Landi et al. 1997).

The density values at the basis of the corona, determined from the fit of radio data are larger by a factor of about 2.5 than those derived from the Si IX measurement reported in Table 3. They also exceed the average values ($logN_e = 8.2 \div 8.35$) in polar coronal holes, reported by Fludra et al. 1999a, 1999b) but they agree very well with those determined from Si IX line ratio by Del Zanna & Bromage 1997 in this same coronal hole (the elephant trunk hole), observed two rotations before. It must be noticed however that Del Zanna & Bromage 1997 and Fludra et al. 1999a, 1999b did not include photoexcitation from photospheric background radiation as a populating mechanism for the Si IX ground levels. Neglecting this process leads to slightly overestimate the electron density.

The discrepancy between the electron density inferred from Si IX and that derived from the fit of radio data can be, at least in part, ascribed to one of the following reasons: *(i)* The regions of the coronal hole where EUV line intensities and radio brightness temperature have been averaged are not the same. and, *(ii)* the scarce angular resolution at low frequencies overestimates the radio brightness temperature in the hole, thus requiring a higher electron density in the corona.

Another serious physical reason of the overestimation of the electron density derived from radio data will be discussed in Sect. 5.

4.2. Synthetic EUV spectra

The three models used to fit the radio data shown in Fig. 5 have been then used to compute the intensity of the EUV lines listed in Table 1: the resulting I_{calc}/I_{obs} ratios are plotted in Fig. 6 as a function of wavelength.

Fig. 6 shows that synthetic EUV intensities of transition region lines are not affected by the choice of the T_c value, while coronal line intensities are very sensitive even to small changes of T_c. For this reason they are able to provide further constraints to the temperature in the coronal hole, which could not be achieved from our radio data, since only an upper limit of T_b at the lowest frequency is available. Fig. 6 shows that the best agreement between theoretical and observed intensities is reached at $T_c = 8.9 \times 10^5$ K, which is consistent with the results obtained from radio data. Moreover, the top panel in Fig. 6 is able to supply a lower limit to the measured coronal temperature: EUV line intensities computed assuming $T_c = 7.9 \times 10^5$ K are in fact too low.

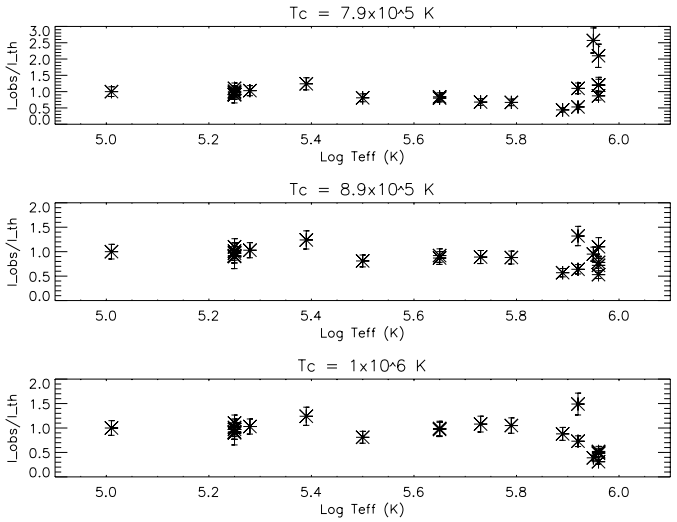

Fig. 6. Comparison between theoretical and observed EUV line intensities.

It must be pointed out that the computed line intensities using both the *DEM* curves shown in Fig. 3, without considering the contribution from an isothermal plasma, are of course in very good agreement with the observations, being the curves derived from the best fit of the observed line intensities. This indicates that, contrary to what we found for radio data, EUV line intensities can be equally well reproduced by an atmosphere with or without an isothermal corona, provided that the upper limit of the *DEM* definition is properly set.

4.3. Reliability of the results

In the present work the new standard CDS intensity calibration (revised in late December 1998) has been used. To evaluate the effect of possible calibration uncertainties in our results, the whole study has been repeated using the old, pre-flight intensity calibration (Bromage et al. 1997), and theoretical radio brightness temperatures have been re-calculated. The differences between the resulting T_b values are negligible, being smaller than 1%.

Similar comparisons have been carried out using different sets of ion fractions (Shull & Steenberg 1982, Mazzotta et al. 1998). Again, differences on the resulting T_b values are negligible.

This means that the results of the present work are not affected by uncertainties neither in EUV intensity calibration nor in the adopted ion fractions.

The accuracy on the radio brightness temperature has been estimated around 5×10^4 K ($\leq 10\%$ of the measured T_b vlaues); moreover, another source of uncertainty in the present study comes from having compared EUV and radio data averaged over two different portions of the hole. In Sect. 2.2 this uncertainty has been estimated to be smaller than 15%: this is the main limitation to the reliability of the results obtained in the present work.

5. Discussion

The obtained results indicate that radio data cannot be fitted without the presence of a corona with a slowly decreasing density and that the crucial parameters in the derivation of the radio spectrum are the *DEM* in the TR and the parameters (N_e, T_e) at the bottom of the corona.

It must be pointed out however, that the coronal contribution to the radio brightness temperature (and also to coronal line intensities) depends on the temperature and on the emission measure, $EM = \int N_e^2 dh$ rather than on the electron density itself. In our case the electron density at the basis of the corona was derived from the best fit of radio data having assumed the corona in hydrostatic equilibrium and getting therefore: $EM = N_e(0)^2\, H/2$ with the scale height given by $H = T_c/\alpha$. The resulting Emission Measure is $EM = 2.7 \times 10^{26}$ cm^{-5}, in agreement with Yohkoh determinations ($logEM = 25.5 \div 26.2$) according to Hara et al. 1994.

The assumption of hydrostatic equilibrium in coronal holes could appear in conflict with the very well established origin of the fast Solar Wind in these coronal features. However, UVCS observations (Kohl et al. 1998) have shown that outflow velocities are negligible below 1.5 $R_\odot$ where no difference is noticed in the electron density profiles between a static and a dynamic coronal model. Similar results have been obtained, using LASCO data (Sheeley et al. 1997, below 2 $R_\odot$).

Since the coronal contribution to the radio brightness temperature at the considered frequencies, as well as that to the EUV line intensities, comes from the deepest layers of the solar corona ($R < 1.05\ R_\odot$), the assumption of hydrostatic equilibrium is fully justified.

On the contrary, the consequences of having assumed the temperature derived from the fit of radio data to determine the coronal scale height are important. In fact the radio emission of the quiet corona is due to thermal bremstrahlung and the corresponding temperature is the electron temperature, while that entering the scale height is an average plasma temperature.

Recent SOHO and Ulysses observations seem to indicate that the proton and the electron kinetic temperatures are quite different, mostly in coronal holes, the latter being much lower than the former. According to Fludra et al. 1999b, the average density profile of several polar coronal holes suggest that $T_p > 2\, T_e$.

If $T_p \gg T_e$, the scale height of the coronal plasma, which must be neutral, depends on the average coronal temperature and is therefore larger than that determined assuming $T_c = T_e$, thus increasing the emission measure, the radio optical depth and hence the T_b. In order to find again a good fit of radio observations we should either decrease T_e or decrease $N_e(0)$ proportionally to $H^{-1/2}$. It has been shown in Fig. 6 that in the former case, it would not be possible to get the correct intensity of EUV lines formed at $T \simeq 10^6$ K, while, in the latter one, no variation would be noticed, since the coronal contribution to the line intensity also depends on $EM = N_e(0)^2 H/2$. In order to have the same EM with $T_p > T_e$ we should decrease the electron density $N_e(0)$ to $N'_e(0)$ according to:

$$N'_e(0) = N_e(0) \times \left(\frac{2\, T_e}{T_p + T_e} \right)^{1/2} \tag{12}$$

Assuming a ratio $\frac{N_e(0)}{N'_e(0)} = 2.5$ between the electron density derived from the fit of radio data and the values measured from Si IX, a proton temperature $T_p \simeq 11 T_e$ is found, providing an average coronal temperature $T_c \simeq 5.6 \times 10^6$ K. This value seems too large and its overestimation is probably due to one of the reasons mentioned in Sect. 4.1.

6. Summary and conclusions

In this paper we have analysed EUV and radio observations of an equatorial coronal hole at its central meridian transit, on October 18 and 19, 1996.

This analysis has shown the very powerful diagnostic provided by these two types of observations, when combined together. Using the *DEM* derived from EUV line intensities in the radio transfer equation and comparing the results with the observed radio brightness temperatures, it is possible to derive the parameters of the solar corona.

It has been shown that EUV line intensities can be equally well reproduced by an atmosphere with or without a corona, by properly changing the top temperature in the *DEM*, while radio data can't.

The best estimate of the coronal electron temperature usually comes from the low frequency observations where $\tau_c \geq 1$ and $T_e \simeq T_b$. Unfortunately, in our case, due to the low angular resolution of the Nançay Radioheliograph at the 164 MHz, as compared with the hole size, only an upper limit, $T_b < 9 \times 10^5$ can be inferred. Any coronal temperature between 8 and 9×10^5 K seem therefore to fit very well the radio observations. The observed EUV line intensities however put a constraint on the lowest acceptable value of the coronal temperature, which has been estimated $T_c = 8.9 \times 10^5$ K.

About the same estimate of the coronal temperature has been given by Del Zanna and Bromage 1997, who analysed the CDS line intensies in this same hole, observed two rotations before. Also David et al. 1998 find a temperature profile increasing from 7×10^5 at $1.05 R/R_\odot$ to $1.\ 10^6$ K at $1.16 R/R_\odot$ as a result of analysis of several EUV lines observed by CDS and SUMER above a polar coronal hole. A similar temperature increase, from $7.6\ 10^5$ to $9.\ 10^5$ K has been found above several polar coronal holes by Fludra et al. 1999a,1999b.

All these results agree with the radio brightness temperature derived in this paper. This removes a long-standing discrepancy between the coronal hole temperature required by the radio and EUV observations. However a discrepancy still exist with the Yohkoh X-ray data (Hara et al. 1994 and reference therein).

The estimate of the electron density at the basis of the corona $N_e(0) \simeq 2.8 \times 10^8$ cm^{-3} at $T_c = 8.9 \times 10^5$ K, also derived from the fit of radio data, depends more crucially on the assumption made in deriving the coronal contribution to T_b (and to the line intensity), namely the hydrostatic equilibrium in the coronal portion of the hole with a scale height $H = T_e/\alpha$. (The

assumptions made on the electron pressure trend in the TR do not seem to influence the results)

It has been shown that the assumption of hydrostatic equilibrium can be safely applied in our case, since the radiation we are considering comes from the very low corona where dynamic effects are negligible.

The assumption of a coronal temperature $T_c = T_e$ can considerably underestimate the real scale height in the corona, thus increasing the estimated value of $N_e(0)$ in order to get EM and τ_c able to account for radio and EUV observations.

It is in our purposes to check, using the present set of data, coronal hole models which assume a difference between electron and proton temperature, necessary to reconcile the requirement of a very low electron temperature, with the high wind speed observed by Ulysses above coronal holes.

Acknowledgements. SOHO is a mission of international cooperation between ESA and NASA. The CDS project is supported by the United Kingdom PPARC. We would like to thank M.Landini for useful discussions and J.M. Delouis for his help in the radio data reduction. We would like to thank also Dr. K. Shibasaki for very useful comments on the original manuscript. One of the authors (EL) acknowledges financial support from the Italian Space Agency (ASI contract RS-96.141).

References

Altshuler M.D., Perry R.M., 1972, Solar Physics 23, 410
Arnaud M., Raymond J.C., 1992, ApJ 398, 394
Arnaud M., Rothenflug R., 1985, A&AS 60, 425
Bromage B.J.I., Breeveld A.A., Kent B.J., Pike C.D., Harrison R.A., 1996, UCLan Report CFA/96/09
Chiuderi Drago F., 1974, In: Righini G. (ed.) SkyLab Solar Workshop, Oss. e Mem. Oss. Astr. Arcetri n., 104
Chiuderi Drago F., Avignon Y., Thomas R.J., 1977, Solar Physics 51, 143
Chiuderi Drago F., Kerdraon A., Landi E., Fludra A., 1999, Space Sci. Rev., in press
David C., Gabriel A.H., Bely-Dubau F., et al., 1998, A&A 336, L90
Del Zanna G., Bromage B.J.I., 1997, Proccedings of the fifth SOHO Workshop, ESA SP-404, 323
Del Zanna G., Bromage B.J.I., 1999, Journal of Geophysical Research, in press
Dere K.P., Landi E., Mason H.E., Monsignori Fossi B.C., Young P.R., 1997, A&AS 125, 149
Dulk G.A., Sheridan K.V., 1974, Solar Physics 36, 191
Feldman, U., Mandelbaum P., Seely J.L., Doschek G.A., Gursky H., 1992, ApJS 81, 387
Fludra A., Del Zanna G., Bromage B.J.I., Thomas R.J., 1997, Proccedings of the fifth SOHO Workshop, ESA SP-404, 385
Fludra A., Del Zanna G., Alexander D., Bromage B.J.I., 1999a, J. Geophysical Res., in press
Fludra A., Del Zanna G., Bromage B.J.I., 1999b, Space Sci. Rev., in press
Grevesse N., Anders E., 1991, In: Cox A.N., Livingston W.C., Matthews M.S. (eds.) Solar Interior and Atmosphere. Univ. Arizona Press, Tucson, 1227
Haisch B., Saba J.L.R., Meyer J.-P., 1996, In: Pallavicini R., Dupree A.K. (eds.) Preceedings of the 9^th Cambridge workshop on Cool Stars, Stellar systems and the Sun. ASP Conf. Series 109, p. 511
Hara H., Tsuneta S., Acton L.W., et al., 1994, PASJ 46, 493
Harrison R.A., Sawyer E.C., Carter M.K., et al., 1995, Solar Physics 162, 233
Kerdraon A., Delouis J-M., 1997, Lecture Notes in Physics, 483
Kohl J.L., Noci G., Antonucci E., et al., 1998, ApJ 501, L127,
Kosugi T., Ishiguro M., Shibasaki K., 1986, PASJ 38, 1
Kundu M.R., 1965, Solar Radio Astronomy. N.Y. Interscience Pub.
Landi, E., Landini M., 1997, A&A 327, 1230
Landi E., Landini M., Pike C.D., Mason H.E., 1997, Sol. Phys. 175, 553
Landi, E., Landini M., 1998, A&A 340, 265
Landi E., Landini M., Dere K.P., Young P.R., Mason H.E., 1999, A&AS 135, 339
Lantos P., Avignon Y., 1975, A&A 41, 137
Mazzotta P., Mazzitelli G., Colafrancesco S., Vittorio N., 1998, A&AS 133, 403
Munro R.H., Withbroe G.L., 1972, ApJ 176, 511
Reeves E.M., Parkinson W.H., 1970, ApJS 21, 1
Sheeley N.R., Wang Y.-M., Hawley S.H., et al., 1997, ApJ 484, 472
Shull J.M., Van Steenberg M., 1982, ApJS 48, 95
UnderwoodJ.H., Muney W.S., 1967, Solar Physics 1, 129
Young P.R., Landi E., Mason H.E., Landini M., 1999, A&A, in preparation